

---

---

---

---

# Metallurgical and Mechanical Properties of Electron Beam Welded AA2219 Aluminium Alloy Joints

<sup>1</sup>S.Malarvizhi\*, <sup>2</sup>V.Balasubramanian and <sup>3</sup>N.Viswanathan

<sup>1,2</sup>Centre for Materials Joining & Research (CEMAJOR), Department of Manufacturing Engineering, Annamalai University, Annamalainagar 608002, Tamilnadu

<sup>3</sup>Department of Engineering, Defence Research & Development Laboratory (DRDL),Kanchanbagh (P.O), Hyderabad.

## ABSTRACT

AA2219 aluminium alloy joints without filler metal addition were produced using electron beam welding (EBW) process. Microstructure characteristics, tensile properties, fatigue strength and fatigue crack growth resistance of the welds were evaluated and presented in this paper.

**Key Words:** AA2219 aluminium alloy, electron beam welding, artificial aging treatment, tensile properties and fatigue performance.

## INTRODUCTION

Aluminium alloy 2219 (Al-Cu-Mn ternary alloy) has excellent cryogenic properties. It has a unique combination of properties such as good weldability and high strength to weight ratio. The preferred welding processes for AA2219 aluminium alloy are gas metal arc welding (GMAW) and gas tungsten arc welding (GTAW) due to their comparatively easier applicability and better economy [1]. Plasma arc welding (PAW) with electrode positive and high welding current allows aluminium components to be joined economically with an excellent weld quality [2]. In comparison with the electric arcs, the electron beam is characterized by a higher power density and thus permits the single pass welding of square butt joints with thickness up to approximately 8 mm in the flat position at welding speeds up to more than 1 m/min. Electron beam welds of most of

the weldable materials including aluminium alloys exhibit superior mechanical properties compared to the welds made using GTAW [3].

Though AA2219 has got an edge over its 6000 and 7000 series counterparts in terms of weldability, it also suffers from poor as welded joint strength[4].

The gap between strength values of the base metal and weld metal, particularly yield strength values, is significantly large, forcing the design engineers to use thicker base metal plates, which in turn increases the total weight of the structure. This fact is of concern in aerospace applications because, use of thicker plates due to low yield strength of the weld metal results in lowering of the payload [5]. Hence, an attempt was made to evaluate microstructure characteristics, tensile properties and fatigue properties of electron beam welded 12 mm thick AA2219 aluminium alloy plates and the results are presented

in this paper.

## EXPERIMENTAL WORK

Plates of AA2219-T87 aluminium alloy of thickness 12 mm were cut to the required dimensions (300 mm x 150 mm x 12 mm) and machined. Table 1 presents the chemical composition and mechanical properties of base metal. Square butt joint configuration, as shown in Fig. 1a, was prepared to produce electron beam (EB) welded joints. The initial joint configuration was obtained by securing the plates in position using tack welding. All necessary care was taken to avoid joint distortion and the joints were made after clamping the plates with suitable clamps. EB welds were produced using an electron beam welding machine (Techmeta, France) with 100 kV capacity. The welding conditions and process parameters used to fabricate the joints are presented in Table 2.

---

---

---

Metallographic specimens were sectioned to the required sizes from the joint comprising weld metal, HAZ and base metal regions and were polished using different grades of emery papers. Final polishing was done using the diamond compound (1  $\mu$ m particle size) in the disc polishing machine. Microstructural examination was carried out using a light optical microscope (Make: Union Optical, Japan; Model: VERSAMET-3) incorporated with an image analyzing software (Clemex-Vision). Specimens were etched with Kellers reagent to reveal the microstructure. As most of the joints failed in the weld metal, this part of the joint was examined using transmission electron microscope (TEM; Make: PHILIPS, Model: CM20). Vicker's microhardness testing machine (Make: Matzusawa, Japan, Model: MMT-X7) was employed for measuring the hardness across the joint with 0.5 kg load.

Transverse tensile specimens were prepared as shown in Fig. 1 as per American Society for Testing of Materials (ASTM) E8M-2004. Smooth (unnotched) tensile specimen (Fig. 1b), was prepared and tensile tests were conducted to determine the tensile properties of the base metal and the weld joints. Notched tensile specimen (Fig. 1c), was prepared and tested to estimate notch tensile strength and notch strength ratio. These tests were carried out in 100 kN, electro-mechanical controlled Universal Testing Machine. The specimen was loaded at the rate of 1.5 kN/min as per ASTM specifications. The 0.2% offset yield strength was derived from the load - elongation diagram.

Hourglass type (smooth) specimens were prepared as shown in Fig. 1(b) from weld joints in the transverse direction to evaluate the fatigue life (S-N behaviour).

Notched specimens were also prepared as shown in Fig. 1(c) from weld joints to evaluate the fatigue notch factor and notch sensitivity factor. The fatigue testing experiments were conducted at different stress levels and all the experiments were conducted under uniaxial tensile loading condition (stress ratio = 0) using servo hydraulic fatigue testing machine (Make: INSTRON, UK; Model:8801). At each condition, five specimens were tested and the test results are used to plot S-N curves.

Centre Cracked Tension (CCT) fatigue crack growth test specimen were prepared to the dimensions as shown in Fig. 1(d). The slices derived from the single pass welded joints were reduced to a thickness of 8 mm by shaping and grinding processes to obtain flat and required surface roughness. Then the sharp notch was machined in the weld region to the required length using the wire cut electric-discharge machine (EDM). Procedures prescribed by the ASTM E647-04 standard were followed for the preparation of the specimens. Fatigue crack growth experiments were conducted using the same machine that was used for fatigue tests with a frequency of 10 Hz under constant amplitude loading ( $R = \text{stress ratio} = \sigma_{\min}/\sigma_{\max} = 0$ ). Fatigue crack growth experiments were carried out at four different stress levels (25 MPa, 50 MPa, 75 MPa and 100 MPa). Before loading, the specimen surface was polished using metallographic procedures and illuminated suitably to enable the crack growth measurement. A traveling microscope, incorporated with a web camera and video output, was used to monitor the crack growth with an accuracy of 0.01 mm. In this investigation, the applied stress cycle was in the tensile mode (the minimum stress was kept at zero) as the

compressive mode usually closes the fatigue crack.

## RESULTS AND DISCUSSION

### Microstructure

Microstructures of the weld base metal and the weld metal as revealed by TEM are shown in Fig. 2. The dislocation cell structure seen at higher magnification is shown in Fig. 3. From the microstructures shown in Fig 2, the following inferences can be obtained:

- (i) There is appreciable difference in the distribution and size of precipitates ( $\text{CuAl}_2$ ) between base metal and weld joints (Fig. 2);
- (ii) Precipitate fraction is less in the weld region (Fig. 2b) than base metal (Fig. 2a) because the precipitates dissolve due to welding heat;
- (iii) The base metal contains very closely spaced, dense dislocation cell structure (Fig. 3a) and this may be due to the prior metal working operations carried out on the material.
- (iv) In the weld region (Fig. 3b) the dislocation cell structure is not seen because of melting and subsequent solidification of this zone

### Microhardness

Appreciable difference in microstructure was obtained on the top surface and cross sectional direction of welded joints and hence hardness was measured on the top surface and cross section of the welded joints. During the microstructure analysis it was observed that the interface region of base metal and weld metal consist of very narrow heat affected zone (HAZ). Within the narrow HAZ, two distinct regions were

---

---

---

observed. They are: (i) Fine grained HAZ (FGHAZ-just adjacent to the weld metal region) and (ii) Coarse grained HAZ (CGHAZ-very close to the base metal region). Hence, the micro-hardness was measured at four different locations (Fig. 4). They are: (i) weld metal (WM), (ii) FGHAZ (iii) CGHAZ and (iv) Unaffected Base Metal (BM). At each of these regions, three readings were taken and average of three readings is presented in Table 4.

Hardness of the base metal in its initial T87 condition is approximately 140 Hv and the hardness of the weld metal is 105 Hv. The base metal contains closely spaced, dense dislocation cell structure and this is because of prior work hardening carried out on the material to attain T87 condition. Both in the weld metal and HAZ, work hardening effect is lost and the precipitates dissolve and this leads to reduction in hardness.

Hardness is relatively higher in the FGHAZ region than WM and this may be due to the formation of very fine recrystallised grains in that region. Hardness of the weld top surface also showed similar trend but there is a reduction of approximately 5-10 Hv compared to cross sectional hardness. This may be largely due to the presence of coarse and elongated grains at the top surface of the welds. Coarse and elongated grains generally will have less grain boundary area compared to fine grains and subsequently will show less resistance to indentation or plastic deformation [6].

### Tensile Properties

The transverse tensile properties such as yield strength, tensile strength, percentage of elongation, percentage of reduction in cross sectional area, notch tensile strength, notch strength ratio and joint efficiency of base metal and

welded joint are presented in Table 5. In each condition, three specimens were tested and the average of three results is presented in Table 5. Fracture of the specimens occurred in the weld region, indicating strength of the joint is less than that of the base metal. The yield strength and tensile strength of unwelded parent metal are 390 MPa and 470 MPa respectively. The elongation and reduction in c.s.a. of unwelded parent metal are 15% and 10.5% respectively. It is clear from the Table 5 that corresponding values estimated from the tensile tests conducted on the transversed weld joint specimens are lower than that obtained for the base metal confirming weld joint is weaker than the base metal.

The notch tensile strength of unwelded parent metal is 437 MPa. But the notch tensile strength of as welded (AW) joint is 319 MPa. This reveals that the reduction in NTS is approximately 30% due to EB welding. Another notch tensile parameter, NSR is found to be less than unity (<1) for unwelded, parent metal of AA2219 aluminium alloy. This suggests that the AA2219 alloy is sensitive to notches and they fall into the 'notch brittle materials' category. The NSR is 0.93 for unwelded parent metal but it is 1.16 for the as welded joints. From the above results, it is very clear that tensile properties of the EB weld joints are inferior to that of the base metal. It is also evident from the hardness of the weld metal and the base metal.

The size and distribution of CuAl<sub>2</sub> precipitates play a major role in deciding the tensile properties and hardness of the EB welds of AA2219 alloy [7]. From the microstructural analysis it is observed that the welded joint invariably consist of very fine, equiaxed grains. There is no evidence of any dendritic solidification. This is mainly due to the very high

solidification rates associated with electron beam welding. Fine evenly distributed CuAl<sub>2</sub> precipitates are the reason for high strength of AA2219 base material. These strengthening precipitates form due to the solution treatment and subsequent artificial aging. During welding, these precipitates dissolve and the weld metal should be left devoid of any precipitates. However, due to the high heating and cooling rates involved in welding [8] not all of them get dissolved and few of them survive in a fine needle shaped precipitates throughout the matrix. Further, after welding, joint cools in air and during this cooling, it is possible that some natural ageing of the alloy takes place. This is in contrast with the cooling by quenching in cold water during the solution annealing treatment. Hence natural ageing of the weld joint could also be one of the reasons for the fine precipitates observed in the weld metal in the as-welded condition.

### S-N Behaviour

Fig.5 shows the fatigue life of unnotched and notched specimens in the form of S-N curves. When comparing the fatigue strength of different welded joints subjected to similar loading, it is convenient to express fatigue strength in terms of the stresses corresponding to particular lives, for example 10<sup>5</sup>, 10<sup>6</sup> and 10<sup>7</sup> cycles on the mean S-N curve. The choice of reference life is quite arbitrary. Traditionally, 2 x 10<sup>6</sup> cycles has been used, and indeed some design codes refer to their S-N curves in terms of the corresponding stress range [9]. For these reasons, in this investigation, fatigue strength of welded joints at 2 x 10<sup>6</sup> cycles was taken as a basis for comparison. The stress corresponding to 2x10<sup>6</sup> cycles was taken as the endurance limit. The endurance limit evaluated for the base metal and welded

joint are presented in Table 6.

The effect of notches on fatigue strength is determined by comparing the S-N curves of notched and unnotched specimens. The data for notched specimens are usually plotted in terms of nominal stress based on the net cross section of the specimen. The effectiveness of the notch in decreasing the fatigue limit is expressed by the fatigue strength reduction factor or fatigue notch factor,  $K_f$ . The fatigue notch factor for the base metal and welded joint was evaluated using the following expression [10] and they are given in Table 6.

$$K_f = \frac{\text{Fatigue limit of unnotched specimen}}{\text{Fatigue limit of notched specimen}} \quad (1)$$

The notch sensitivity of a material in fatigue is expressed by a notch sensitivity factor 'q' and 'q' can be evaluated using the following expression [10]

$$q = \frac{(K_f - 1)}{(K_t - 1)} \quad (2)$$

where  $K_t$  is the theoretical stress concentration factor and is the ratio of maximum stress to nominal stress. Using the above expression fatigue notch sensitivity factor 'q' was evaluated for base metal and welded joint and they are presented in Table 6.

The fatigue strength of the base metal, AA2219 aluminium alloy is 200 MPa. But the fatigue strength of as-welded (AW) joint is 150 MPa. This indicates that there is a 25% reduction in fatigue strength joints from that of the base metal. Fatigue notch factor of unwelded AA2219 aluminium alloy is 1.82; but the fatigue notch factor of as welded (AW) joint is 2.73. This indicates that there is a 50% increase in fatigue notch factor value for the joints. Similar trend was observed in notch sensitivity factor values also since it was derived using

fatigue notch factor values. Generally, if the fatigue notch factor is lower, then the fatigue life of the joints will be higher and vice versa.

### Fatigue Crack Growth Behaviour

The measured variation in crack length (2a) and the corresponding number of cycles (N) endured under the action of particular applied stress range are plotted as shown in Fig.6 for base metal and welded joint. The fracture mechanics, based Paris Power equation [11] given below, was used to analyze the experimental results.

$$da/dN = C (\Delta K)^m \quad (3)$$

where, da/dN - crack growth rate,  $\Delta K$  - stress intensity factor (SIF) range, 'C' and 'm' are constants.

The SIF value was calculated for different values of growing fatigue crack length '2a' using the following expression [12]

$$\Delta K = (\Phi) (\Delta \sigma) \sqrt{La} \quad (4)$$

However, the geometry factor ' $\Phi$ ' for the CCT specimen was calculated using the expression given below [12]

$$\Phi = F(\alpha) = \sec\left\{\frac{\alpha}{2}\right\} \quad (5)$$

Where  $\alpha = a/W$

The crack growth rate, da/dN for the propagation stage was calculated for the steady state growth regime, at different intervals of crack length increment. The relationship between SIF range and the corresponding crack growth rate in terms of best fit lines is shown in Fig. 7. The data points plotted in the graph mostly correspond to the second stage of Paris sigmoidal relationship ( $10^{-6}$  to  $10^{-3}$  mm/cycle). The exponent 'm', which is the slope of the line on log-log plot and the intercept 'C' of the line was determined and they are presented in Table 7. When the crack growth rate is

around  $10^{-3}$  mm/cycle, the curve tends to become parallel to the Y-axis and the corresponding  $\Delta K$  value is taken as critical SIF range ( $\Delta K_{cr}$ ). At lower values of  $\Delta K$ , around  $10^{-6}$  mm/cycle, the curve again becomes parallel to the Y-axis, indicating a threshold SIF ( $\Delta K_{th}$ ) below which a crack may not propagate. The values of  $\Delta K_{cr}$  and  $\Delta K_{th}$  for base metal and welded joint were evaluated and are presented in Table 7.

The crack growth exponent 'm', which was derived from the relationship existing between crack growth rate (da/dN) and SIF range, is an important parameter to evaluate the fatigue crack growth resistance of materials since it decides the fatigue crack propagation life of the materials. This exponent was obtained from the slope of the curve drawn between da/dN and SIF range. If this exponent is lower, then slope of the curve is lower and that indicates the resistance offered by the material to the growing fatigue crack is higher and hence the fatigue life will be longer. If this exponent is larger, then slope of the curve is higher and that explains the resistance offered by the material to the growing fatigue crack is lower and hence the fatigue life will be shorter [13]. The fatigue crack growth exponent of AA2219 aluminium alloy is 2.79. But the fatigue crack growth exponent of as welded (AW) joint is 4.10. This indicates that there is a 45% increase in fatigue crack growth exponent value due to EB welding.

From the fatigue test results (Table 6) and the fatigue crack growth test results (Table 7), it is found that the weld joint exhibited lower fatigue performance compared to base metal. Reasons for the inferior fatigue performance of the weld joint are: (i) inferior tensile properties of the welded joint and (ii)

microstructural changes in the joint region (iii) unfavorable residual stress pattern in the weld region. Mechanical properties (yield strength, tensile strength and elongation) of welded joint are inferior to those of base metal (see Table 5). Lower yield strength and tensile strength of the weld joint greatly reduce the endurance limit of weld and hence the fatigue crack initiation is fast. Lower elongation (lower ductility) of the welded joint reduces resistance to fatigue crack propagation and hence fatigue crack growth rate is comparatively faster. The combined effect of lower yield strength and lower ductility of the welded joint offered less resistance to crack initiation and crack propagation and hence the fatigue performance of the welded is inferior compared to base metal.

In the CCT specimen, the notch is machined in the weld region of EB welded joints by wire cut EDM (electric discharge machining) process to evaluate the crack growth behaviour of the weld region under fatigue loading. The fatigue crack initiates from the tip of the machined notch and it grows in the weld region until final fracture takes place and hence the weld region microstructure will have an influence on fatigue performance of the joints. Uniformly distributed, very fine particles might have impeded the growing fatigue cracks and hence the fatigue crack growth rate has been delayed (Donnelly and Nelson, 2002) and subsequently the resistance to the fatigue crack propagation has been enhanced compared to weld joint. The weld joint contains very few precipitates and the precipitate free zone is larger. This reduces the resistance of the weld against fatigue crack growth.

The magnitude of residual stress in the

weld region is usually tensile. The tensile residual stress will accelerate the growing fatigue cracks. But the base metal, which was made by rolling method, usually contains compressive residual stress field. The compressive residual stress will decelerate the growing fatigue cracks [15]. This may be the one of the reasons for the inferior fatigue performance of welded joint.

### CONCLUSIONS

- a) The tensile strength and fatigue crack growth resistance of AA2219 aluminium alloy are greatly deteriorated by electron beam welding process.
- b) Electron beam welded joints exhibited a reduction of 40% in tensile strength and 25% in fatigue strength compared to the base metal.
- c) The formation of finer grains, partial dissolution of precipitates, disruption of dislocation cell structure, higher magnitude of tensile residual stress field at the weld region are the main reasons for inferior mechanical and metallurgical properties of electron beam welded joints compared to the base metal.

### REFERENCES

1. Dance G.I (1994) Comparative evaluation of mechanical properties of TIG, MIG, EBW and VPPA welded AA2219 aluminum alloy, *Welding and Metal Fabrication*, Vol.24, pp.216-222.
2. Hartman, J.A., Beil R.J. and Hahn G.T. Effect of copper rich regions on tensile properties of VPPA weldments of 2219-T87 aluminum,

*Welding Journal*,1987, 73-83s.

3. Malarvizhi, S and Balasubramanian, V (2010) Effects of welding processes and post weld aging treatment on fatigue behavior of AA2219 aluminium alloy joints, *Journal of Materials Engineering & Performance* DOI: 10.1007/s11665-010-9682-5.
4. Ishchenko A. Ya, A.V Lozovskaya and I.M.I Sayenko (1989) Fracture Resistance of Aluminium joints in high strength Aluminium alloys under conditions of rapidly increasing load, *Welding international*, 8, 654-656.
5. Kou S and Y. Le (1983) Dendrite morphology in Aluminium alloy welds, *Metallurgical Transactions*, 14 A, 2243-2249.
6. Koteswara Rao S. R., Madhusudhana Reddy, G., Srinivasa Rao, K., Kamaraj, M. and Prasad Rao, K. Reasons for superior mechanical and corrosion properties of 2219 aluminum alloy electron beam welds, *Materials Characterization*, 2006, 40, 236-248.
7. Huang C and S. Kou (2004) Liquefaction cracking in Full penetration Al-Cu welds, *Welding Journal*, 83, 50s - 58s.
8. Garland J.G (1974) Weld pool solidification control, *British Welding Journal*, 22, 121-127.
9. Maddox S.J (2003) Review of fatigue assessment procedures for welded aluminium structures, *International Journal of Fatigue*, pp (1359-1378)
10. Dieter.G.E. (1988) *Mechanical Metallurgy*, 4th ed., Tata McGraw Hill, New York.
11. Guha B (1995) A new fracture mechanics method to predict the

- fatigue life of welded cruciform joints, Engineering Fracture Mechanics, 52, 215-229.
12. Hobbacher A (1996) Recommendations for fatigue design of welded joints and components, IIW Doc., No. IIW - XIII - 1539-96 / XV - 845-96.
  13. Mayer H, M. Papakyriacou, R. Pippen and S. Stanzl-Tschegg (2001) Influence of loading frequency on the high cycle fatigue properties of Al-Zn-Mg-Cu 1.5 aluminium alloy, Material Science and Engineering A, 314, 48-54.
  14. Donnelly E and Nelson D (2002) A study of small crack growth in aluminium alloy 7075 - T6, International Journal of Fatigue, 24, 1175-1189.
  15. Ma T (1999) Softening behaviour of Al-Zn-Mg alloys due to welding, Material Science and Engineering, 266, 198-204.

**Table 1 : Chemical composition (wt%) of base metal**

Type of Material	Cu	Mn	Fe	Zr	V	Si	Ti	Zn	Al
Base Metal (AA 2219-T87)	6.33	0.34	0.13	0.12	0.07	0.06	0.04	0.02	Bal

**Table 2 : Mechanical properties of base metal**

Yield Strength (MPa)	Ultimate Tensile Strength (MPa)	Elongation (%)	Reduction in cross sectional area (%)	Vickers Hardness (0.05 kg) VHN
390	470	15	10.5	140

**Table 3 : Welding conditions and process parameters for EBW process**

Parameter	Value
Current	:: 51 mA
Voltage	:: 50 kV
Speed	:: 16 mm/sec
Gun to work distance	:: 298 mm
Vacuum	:: 10 <sup>-4</sup> bar

**Table 4 : Hardness of different regions of the weld joint**

Locations	WM	FGHAZ	CGHAZ	BM
Cross-section	105	115	110	140
Top surface	100	110	105	134

**Table 5 : Transverse tensile properties of the parent metal and weld joint**

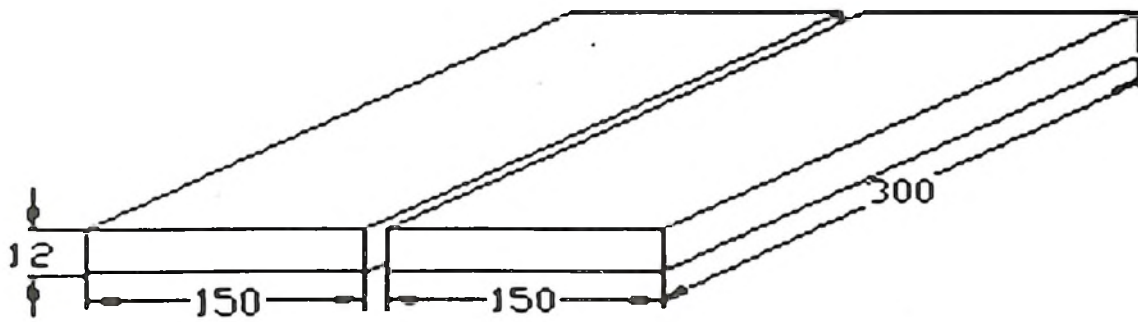
	Yield strength (MPa)	Ultimate tensile strength (MPa)	Elongation (%)	Reduction in cross sectional area (%)	Notch tensile strength (MPa)	Notch strength ratio (NSR)	Joint Efficiency (%)
Base Metal (BM)	390	470	15	10.5	437	0.93	---
Welded Joint (AW)	215	275	9.0	6.2	319	1.16	59

**Table 6 : Fatigue properties of the base metal and weld joint**

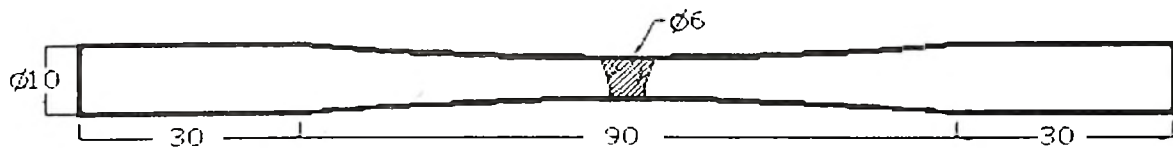
	Fatigue limit of unnotched specimens at $2 \times 10^6$ cycles (MPa)	Fatigue limit of notch specimens at $2 \times 10^6$ cycles (MPa)	Fatigue notch factor (K)	Notch sensitivity factor (q)
Base Metal (BM)	200	110	1.82	0.33
Weld Joint (AW)	150	55	2.73	0.69

**Table 7 : Fatigue crack growth parameters**

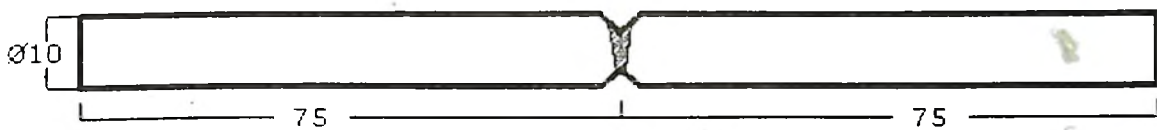
	Crack growth exponent 'm'	Intercept 'C'	Threshold SIF range, $\Delta K_{th}$ (MPa $\sqrt{m}$ )	Critical SIF range, $\Delta K_c$ (MPa $\sqrt{m}$ )
Base Metal (BM)	2.79	$3.5 \times 10^{-8}$	3.50	35
Weld Joint (AW)	4.10	$1.33 \times 10^{-8}$	3.00	15



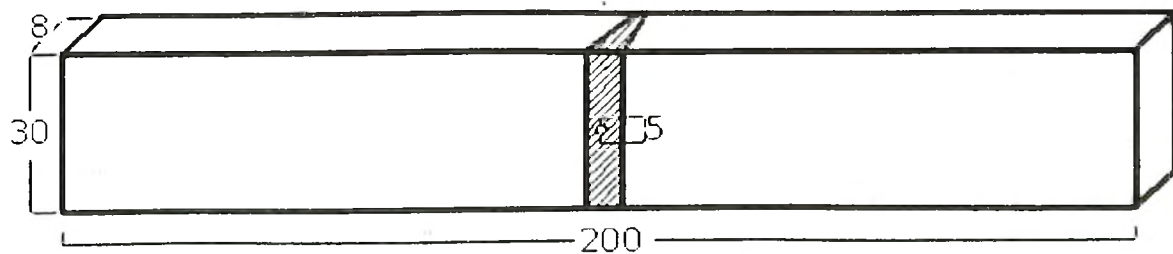
(a) Dimensions of square butt joint prepared in this investigation



(b) Unnotched Tensile / Fatigue Specimen

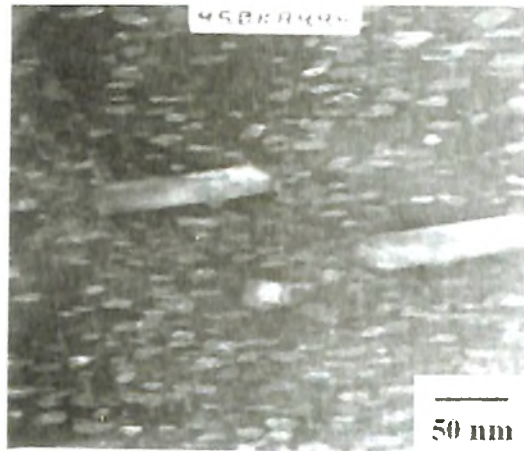


(c) Notched Tensile / Fatigue Specimen

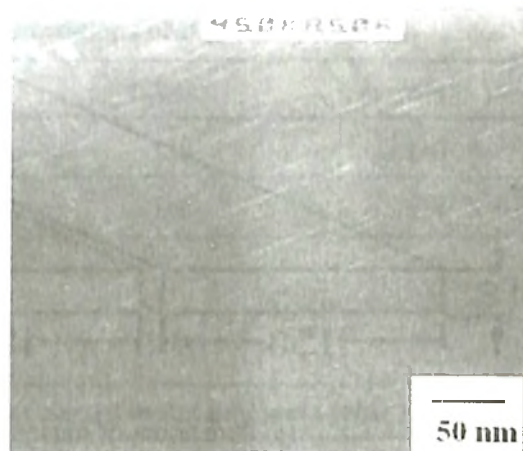


(d) Centre Cracked Tensile Specimen

Fig. 1 : Dimensions (in mm) of various test specimens

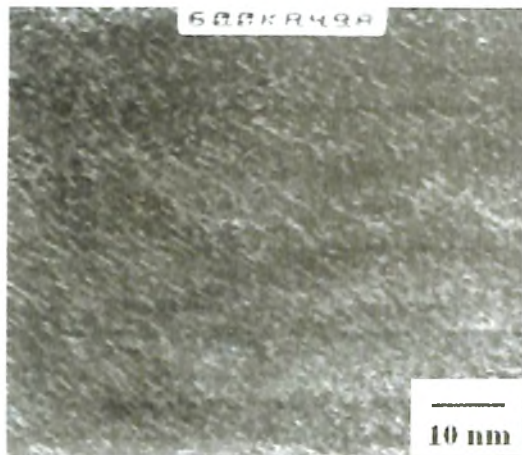


(a) Base Metal

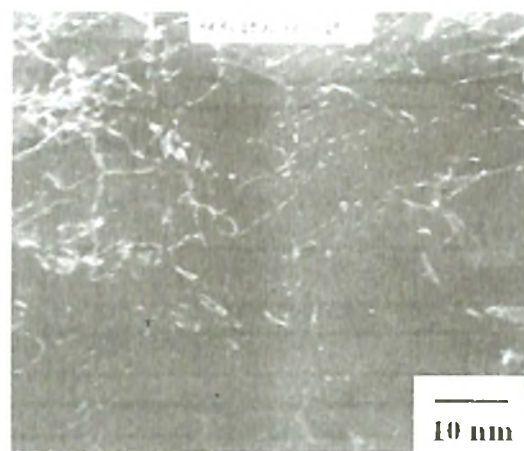


(b) As Welded (AW) Joint

Fig. 2 : Transmission electron micrographs of base metal and weld region

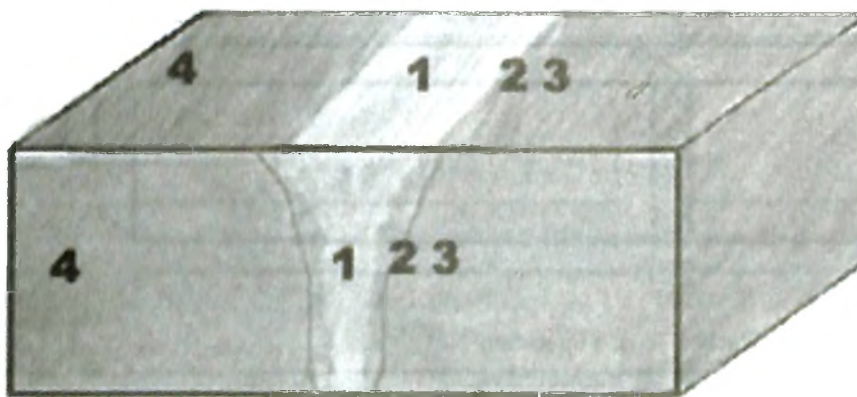


(a) Base Metal,



(b) As Welded (AW) Joint

Fig. 3 : Dislocation cell structure at base metal and weld region



1. Weld metal (WM) region
2. Fine grain HAZ (FGHAZ)
3. Coarse grain HAZ (CGHAZ)
4. Base metal (BM) region

Fig. 4 : Locations of hardness measurement

